ACS APPLIED MATERIALS & INTERFACES

Research Article

www.acsami.org

3D Silver Nanoparticles Decorated Zinc Oxide/Silicon Heterostructured Nanomace Arrays as High-Performance Surface-Enhanced Raman Scattering Substrates

Jian Huang,[†,‡] Feng Chen,[‡] Qing Zhang,[‡] Yonghua Zhan,[⊥] Dayan Ma,*[,†] Kewei Xu,*[,†,§] and Yongxi Zhao*[,‡]

[†]State Key Laboratory for Mechanical Behavior of Materials, School of Materials Science and Engineering, Xi'an Jiaotong University, Xi'an, Shaanxi 710049, People's Republic of China

[‡]Key Laboratory of Biomedical Information Engineering of Education Ministry, School of Life Science and Technology, Xi'an Jiaotong University, Xi'an, Shaanxi 710049, People's Republic of China

[⊥]School of Life Sciences and Technology, Xidian University, Xi'an, Shaanxi 710071, People's Republic of China

[§]Xi'an University, Xi'an, Shaanxi 710065, People's Republic of China

Supporting Information

ABSTRACT: Three-dimensional (3D) hierarchical nanostructures have been considered as one of the most promising surface-enhanced Raman spectroscopy (SERS) substrates because of the ordered arrangement of high-density hotspots along the third dimension direction. Herein, we reported a unique 3D nanostructure for SERS detection based on silver nanoparticles (AgNPs) decorated zinc oxide/silicon (ZnO/Si) heterostructured nanomace arrays. They were prepared by two steps: (1) Si nanoneedles were grafted onto ZnO nanorod arrays via a catalyst-assisted vapor−liquid−solid (VLS) growth mechanism. (2) AgNPs were rapidly immobilized on the surface of nanomaces by a facile galvanic displacement reaction. The fabricated substrates were employed to detect rhodamine 6G (R6G) with a detection limit down to 10^{-16} M, and exhibited a high-enhanced performance (enhancement factor (EF) as high as 8.7×10^7). To illustrate the potential value of the prepared substrates, the different concentrations of melamine aqueous solution (from 10^{-4} to 10^{-10} M) were detected, and a quantitative relationship between the SERS spectrum intensity and the melamine concentration had been established. In addition, the measure of melamine residual in pure milk was carried out successfully, and the results indicated that the prepared 3D nanomace substrates had great potential in food inspection, environment protection, and a few other technologically important fields.

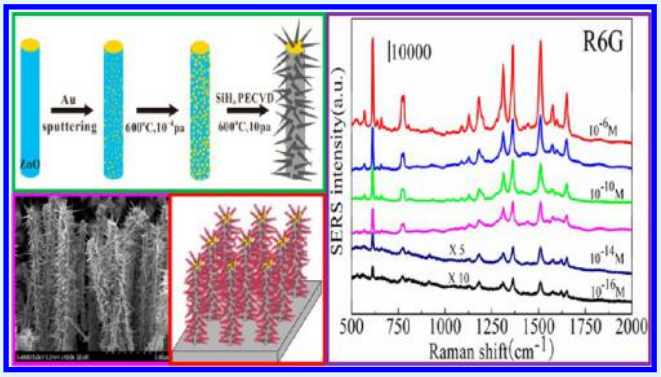

KEYWORDS: *zinc oxide/silicon, nanomace arrays, surface-enhanced Raman scattering, melamine detection*

1. INTRODUCTION

Surface-enhanced Raman scattering (SERS) has been considered as an efficient and powerful analytical technique to detect molecules on or near the surface of plasmonic nanostructures since its discovery in the 1970s.[1] With the combination of high sensitivity, rapid response, and noninvasive analysis, it is widely used for trace-level molecule detection, especially in biochemistry and life sciences.[2−4] For practical applications, it is desired for a robust SERS substrate to possess not only high-density hotspots to ensure high sensitivity but also the uniform distribution of hotspots to achieve good signal reproducibility. To date, extensive efforts have been devoted to fabricate various nanostructures for SERS substrates, such as zero-dimensional (0D) clusters (Au or Ag nanospheres, nanocubes[5,6]), 1D building block (nanowires,[7] nanorods,[8−10] nanotips[11]), 2D planar substrates (nanoplates,[12] rough metal surface[13]), and 3D frameworks (nanoarrays,[14] dendrites,[15,16] nanoflowers,[17−19] branched nanotrees,[20,21] nanobutterfly wing[22,23]). Among them, 3D nanostructures with well controlled hierarchical morphologies have attracted considerable attention.[24,25] Compared with other conventional SERS substrates, 3D nanostructures are far superior due to the fact that they have the potential to further expand the arrangement of hotspots along the third dimension, which could in turn increase the hotspot density.[26,27] In addition, the 3D substrates can also supply larger surface area for adsorbing more probe molecules.

Generally, there are two principal strategies for fabricating 3D hierarchical SERS substrates. The first one is the 3D self-

Received: November 10, 2014
Accepted: March 3, 2015
Published: March 3, 2015

DOI: 10.1021/am507857x
ACS Appl. Mater. Interfaces 2015, 7, 5725−5735

assembly method, which suffers from poor control and reproducibility.[28] Another one is the template method, which consists of noble-metal nanoparticles (NPs) and their 3D nanoscaffolds. Currently, many emerging 3D SERS substrates have been widely reported by the template method. For example, the Au or AgNPs decorated anodic aluminum oxide (AAO) channels,[29] carbon nanotubes (CNTs),[30] titanium dioxide (TiO_2) nanoarrays,[31] zinc oxide (ZnO) nanorod arrays, and so on.[32,33] Nevertheless, the vertical channels (e.g., AAO, CNTs) and aligned nanowire arrays (e.g., TiO_2, ZnO nanoarrays) were unsuitable for the massive amounts of loading of noble-metal NPs and the formation of high-density hotspots. Besides, light propagation is limited owing to significant scattering and adsorption on pore walls and closed pores, which restricted the enhancement efficiency to relatively low levels.[34] To overcome these weaknesses, a promising route is the graft of the vertical channels or aligned arrays (e.g., ZnO nanorod arrays). The uniform spatial distribution of the branched scaffolds can endow the ZnO nanorod arrays with improved sensitivity and reproducibility.

In recent years, ZnO nanorod arrays have been exploited as a universal backbone in an assortment of applications,[35−38] and the graft of aligned ZnO nanorod arrays has also attracted enormous attention. For instance, a new kind of ZnO/CuTCNQ nanotree arrays (TCNQ = 7,7,8,8-tetracyanoquinodimethane) is synthesized through the chemical vapor deposition (CVD) route.[39] However, this route is only able to produce low-density cylindrical branches, and the organic CuTCNQ branches are unsuitable for the loading of noble-metal NPs. Therefore, it is still of urgent need to find applicable branches for the graft of the aligned ZnO nanorod arrays. Recently, a class of silicon nanomaterials has also been reported as an excellent SERS platform by He's group,[40] owing to its biocompatibility, stable chemical properties, and efficient quenching of the interfering excited state luminescence.[41,42] Moreover, huge surface-to-volume ratios of silicon nanomaterials are responsible for their unique optical, mechanical, or electronic properties, which offer exciting opportunities for the design of high-performance SERS substrates.

Inspired by these works and the mace structure, herein, we report a unique substrate for SERS detection based on the graft of Si nanoneedles onto ZnO nanorod arrays and the subsequent decoration of the AgNPs. First, the Si nanoneedles were grafted onto the surface of ZnO nanorod arrays using a catalyst-assisted vapor−liquid−solid (VLS) growth mechanism by reseeding the backbone surface with AuNPs. This method utilizes the loss and shrinkage of catalyst droplet in plasma enhanced chemical vapor deposition (PECVD) and grafts the Si nanoneedles onto the ordered ZnO nanoarrays successfully. Compared with the hydrothermal growth or CVD route, it is less-costly, environmentally friendly and easily suited for industrial production. Second, AgNPs were immobilized on the surface of ZnO/Si nanomace scaffolds via a facile galvanic displacement reaction. By embedding AgNPs on the backbones and branches, the novel 3D SERS substrate is realized. Finally, the AgNPs decorated ZnO/Si 3D hierarchical nanomace arrays were employed as SERS substrates for rapid detection of rhodamine 6G (R6G), with astonishing sensitivity (10^{-16} M) and high Raman enhancement (EF, 8.7×10^7). Additionally, measures of melamine aqueous solution and melamine residual in pure milk were carried out, and the results indicated that the prepared 3D nanomace substrates have great potential in food inspection, environment protection, and other potential applications.

2. EXPERIMENTAL SECTION

Chemicals. Silver nitrate was purchased from Xi'an Dayu Chemicals Industry; hydrofluoric acid was purchased from Dongjiang Chemicals Company; silicon wafers were purchased from Luoyang Single Crystal Silicon Company; silane was purchased from Nanjing Specialty Gas Company; R6G was purchased from J&K Chemical in Beijing; ZnO powder was purchased from Hongtai factory in Yantai; graphite powder was purchased from Chenyang factory in Qingdao. All chemicals were used as received, without further purification. Milk was purchased from a general store in China with a cost of ∼0.4$ per pack. Milli-Q water (>18.0 MΩ cm) was used throughout the experiments.

Fabrication of ZnO/Si 3D Hierarchical Nanomace Arrays. ZnO nanorod arrays were prepared by a bottom-up growth process (based on VLS growth mechanism), which was conducted inside a tube furnace system. The silicon wafer was used as the growth substrates, and a mixed powder (ZnO and graphite powder, mass ratio 1:1) was used as the source material for the VLS growth. The mixed powder was placed in an alumina boat that was then inserted at the center of an alumina tube, where the temperature was set at 950 °C. Argon (flow rate: 160 sccm) was used as the carrier gas to transport zinc vapor to the growth zone. Subsequently, the zinc vapor met and reacted with oxygen (flow rate: 6−8 sccm) to form ZnO vapor species that fed the growth of ZnO nanorod arrays. The pressure of the system was held at 80 Pa, and the growth time varied from 5 to 45 min. Next, Si nanoneedles were grafted onto the surface of ZnO nanorod arrays by the PECVD process adopted by a previous study.[43] The nanorod arrays were coated with a ∼10 nm thick gold layer by ion spurting prior to the PECVD growth. Then, it was placed in a reaction chamber, where the temperature was set at 600 °C. Hydrogen (flow rate: 20 sccm) was used as the carrier gas to transport silane (flow rate: 20 sccm) to the reaction zone. The power of radio frequency (RF) was set at 30 W, the deposition pressure was held at 40 Pa, and the deposition duration varied from 15 to 60 min.

AgNPs Decorated ZnO/Si Hierarchical Nanomace Arrays. AgNPs were deposited on the ZnO/Si hierarchical nanomace arrays by a facile galvanic displacement. First, the as-prepared ZnO/Si 3D nanostructures were immersed into 5% hydrofluoric acid solution for 2 min (obtain the hydrogen passivation surface). Then, dip the chip into silver nitrate solution for 1 min. The silver ions, which adsorb to the Si nanoneedles, were reduced on the hydrogen passivation surface at the same time. Lastly, the samples were carefully washed with deionized water and then dried by N_2 flow for further applications.

Characterization. The morphology and the structure of the as-fabricated 3D hierarchical nanomace arrays were characterized by field emission scanning electron microscopy (FE-SEM, Hitachi SU6600), transmission electron microscopy (TEM, JEM-2100F (JEOL)), and X-ray diffraction (XRD, Bruker D8 Advanced) with Cu Kα radiation. Ultraviolet−visible (UV−vis) spectra were performed on a Hitachi U-4100 spectrophotometer.

SERS Measurements. Raman measurements were performed at room temperature on a Horiba HR 800 Raman system. The 633 nm radiation from an Ar ion laser was used as the excitation source. The laser spot area was ∼1 μm in diameter and the incident power was 1.7 mW. The data acquisition time was 10 s for one accumulation. R6G and melamine were selected as the probe molecule for SERS measurement. When the concentration of R6G within the range of 10^{-12} to 10^{-16} M (including 10^{-12} M), 1 mL of R6G solution was drop-evaporated in ten 0.1 mL portions onto the substrates (the nanomace SERS substrate was tailored into 2 × 3 mm), which were then dried under ambient conditions before tests.[26] The reproducibility evaluation was carried out at six randomly chosen spots from three SERS substrates. Supposing R6G molecules were uniformly distributed on the substrates. All these 6×10^6 R6G molecules (1 mL of 10^{-14} M R6G solution) were adsorbed evenly onto the 6 mm^2 area,

DOI: 10.1021/am507857x
ACS Appl. Mater. Interfaces 2015, 7, 5725−5735

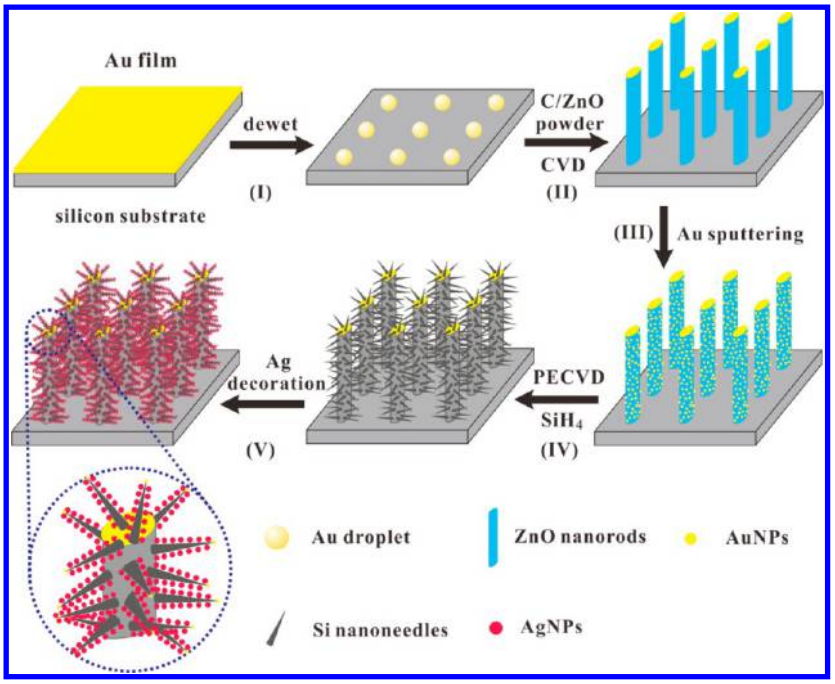

Figure 1. Schematic illustration of the synthesis process of 3D hierarchical ZnO/Si nanomace SERS substrates: (I) dewet gold film; (II) form ZnO nanorod; (III) depositing AuNPs on the ZnO nanorods surface; (IV) growth of Si nanoneedles branch; (V) AgNPs were deposited on the surface of the Si nanoneedles.

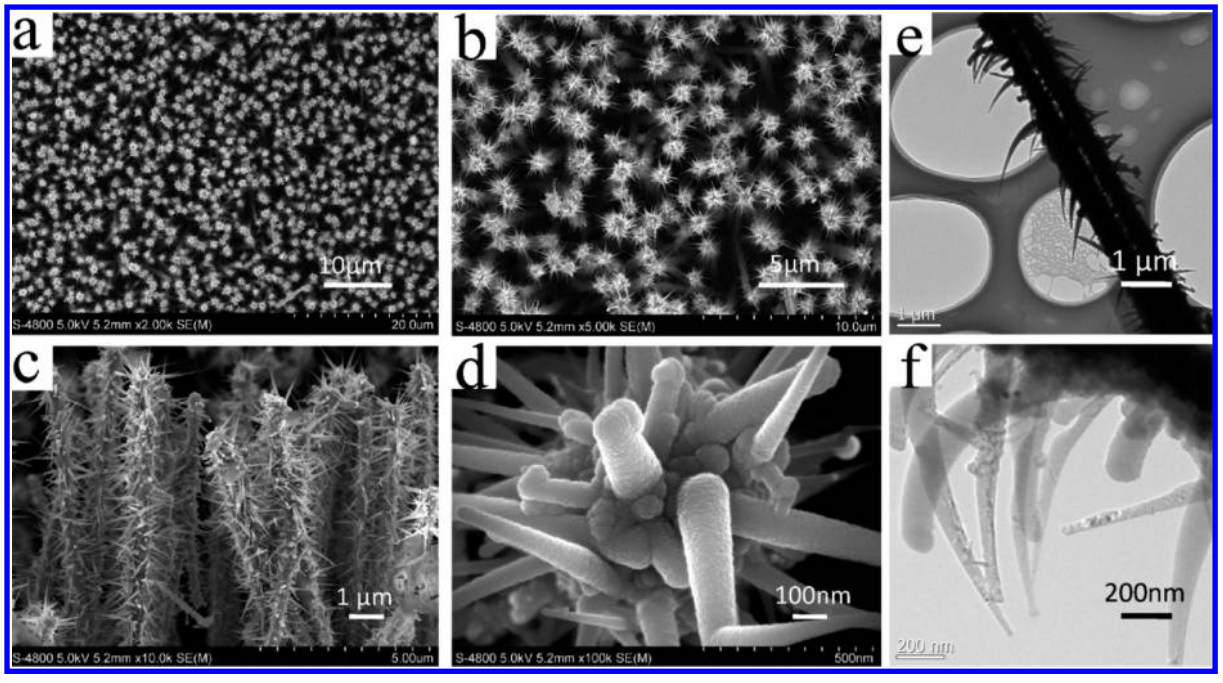

Figure 2. SEM and TEM images of the ZnO/Si nanomace arrays, (a,b,d) top view at different magnifications, (c) side view, and (e,f) different magnifications of TEM images.

the molecular signals collected for Raman measurement were thus from less than ten molecules.

When the concentration of R6G ranged from 10^{-6} to 10^{-12} M, a more convenient method was provided for Raman measurements. 10 μL of R6G solution (from 10^{-6} to 10^{-12} M, respectively) was dropped onto nanomaces substrates with an area of 1 cm^2, and was dispersed to a circular shape area. For example, in our experiments, the dispersed circular shape area was about 10 to 15 mm^2. The concentration of R6G in solution was varied in a wide range by sequential dilution. A similar procedure was applied for other compounds studied here as well. The Raman band of a silicon wafer at 520 cm^{-1} was used to calibrate the spectrometer. It should be noted that the accumulation times and the laser power are the same for all the Raman spectra.

3. RESULTS AND DISCUSSION

3.1. Preparation of 3D ZnO/Si Nanomace Arrays and the Adjustment of Branches. Figure 1 illustrates the fabrication procedure of the 3D hierarchical nanomace SERS substrates. And the procedure was divided into five steps. First, a silicon wafer (5 × 5 cm) was coated with 10 nm gold film as the catalyst before being placed inside a horizontal tube furnace.

DOI: 10.1021/am507857x
ACS Appl. Mater. Interfaces 2015, 7, 5725−5735

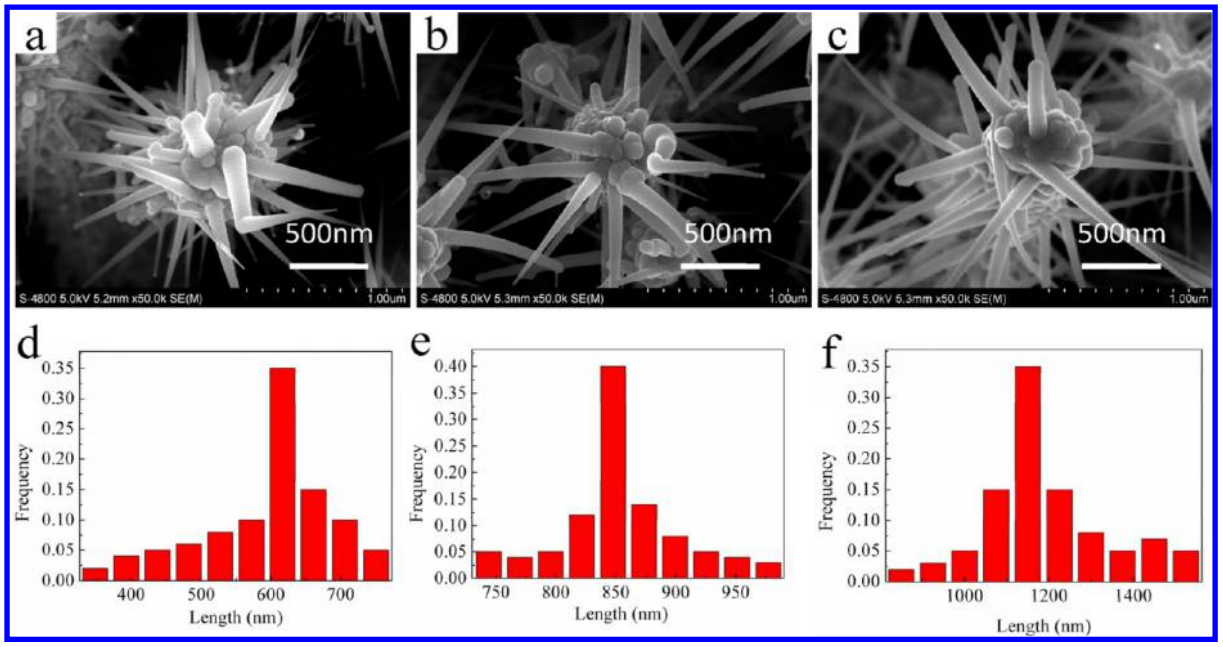

Figure 3. Growth manipulation of the ZnO/Si nanomace arrays by using different deposition durations in PECVD process: (a) 15 min, (b) 30 min, and (c) 45 min. The histogram (d,e,f) under each panel represents the length of the branches, respectively.

Upon heating at 873 K, the gold film partially dewet, forming Au/Si droplets on the surface of Si substrate (step I in Figure 1).[44] Meanwhile, the ZnO and graphite powder located at the furnace center can be efficiently evaporated to feed the ZnO nanorods growth by VLS process (step II). In this process, the alloy droplets, acting as a catalytic site for preferential absorption and crystallization of vapor phase reactant, was a vital key to synthesis the ZnO nanorod. This process transformed the flat Si−Au film into aligned ZnO nanorods arrays, and defined the height and interdistance of the backbones (with a height of 5−8 μm at an interval of about 1 μm). Subsequently, the prepared ZnO nanorods arrays were coated with Au seed before being placed inside a PECVD system (step III). As the temperature rises, the liquid catalytic droplets were formed on the surface of ZnO nanorods. A dilute mixture of silane in hydrogen was initiated with a radio frequency power, which results in the pyrolysis of the silane and the initiation of SiH_x cluster growth (step IV). Upon supersaturation of the liquid, the SiH_x precipitated at the liquid−substrate interface, and the nanoneedles grew in a layer-by-layer process.[45] As expected, the Si nanoneedles were successfully prepared on the surface of ZnO nanorods by PECVD. In our experimental conditions, the size of Au−Si droplet gets smaller and smaller owing to the loss and shrinkage that leads to gradual tapering nanoneedles taking place. Prior studies have shown that tapered Si nanowires were grown in an ultrahigh vacuum CVD system as a result of the shrinking seed.[44] Finally, AgNPs were deposited on the surface of backbones and branches by a galvanic displacement reaction (step V, the Si nanoneedles act as a reducing agent for the reduction of silver ions in the solution). The five step procedure is reliable and enables us to fabricate the 3D hierarchical AgNPs decorated ZnO/Si nanomace arrays with high uniformity and good reproducibility.

Figure 2 shows the scanning electron microscopy (SEM) and transmission electron microscopy (TEM) images of the as-prepared ordered ZnO/Si nanomace arrays. The ZnO nanorods are smooth and oriented perpendicular to the substrate surface with excellent uniformity that is consistent with most of previous reports.[46,47] Once the graft of backbones was achieved in PECVD process, the initially smooth ZnO nanorods branched out to form a mace-like nanostructure. It is quite clear that this step generates homogeneous nanomace branches and enhances the loading capacity of the ZnO nanorod scaffolds significantly. The typical images of such structures shown in Figure 2a,b,d represent the top view at different magnifications and panel c represents the side view. Higher magnification of a single nanomace was carried out under TEM, shown in Figure 2e,f, where the silicon nanoneedles show cone-like morphology with a typical branch length from ∼300 to ∼700 nm. The bottom diameter of Si nanoneedle is about 150 nm and gradually decreases from the root to the tip which attributes to the loss and shrinkage of the Au−Si droplet. This is in agreement with previous studies about the preparation of needle-like Si nanowires.[44]

Furthermore, the length of branched Si nanoneedles can be effectively controlled via several means. It is very urgent to increase the length of the branches to enhance the surface area and the loading capacity of the 3D nanomaces arrays. According to Fan's work,[48] the cylindrical ZnO branch structures were grafted onto the Si backbones via a complicated hydrothermal process in organic aqueous solution. And the length of the branches was adjusted only by the growth time (1−5 h). In comparison, the branched Si nanoneedles can be controlled by many different means in our PECVD process, such as working pressure, source gas flow rate, bias voltage, and deposition duration.

Here, deposition duration was considered as a general experimental parameter for the extension of the branches. Three samples with different deposition duration were prepared (from 15 to 45 min), and each sample was characterized by SEM. As shown in Figure 3a, a small amount of short Si nanoneedles emerged from the backbone during the initial growth stage. After 30 min, longer branches were obtained (Figure 3b). By increasing the growth time to 45 min, the backbone's surface was composed of regions with much longer

DOI: 10.1021/am507857x
ACS Appl. Mater. Interfaces 2015, 7, 5725−5735

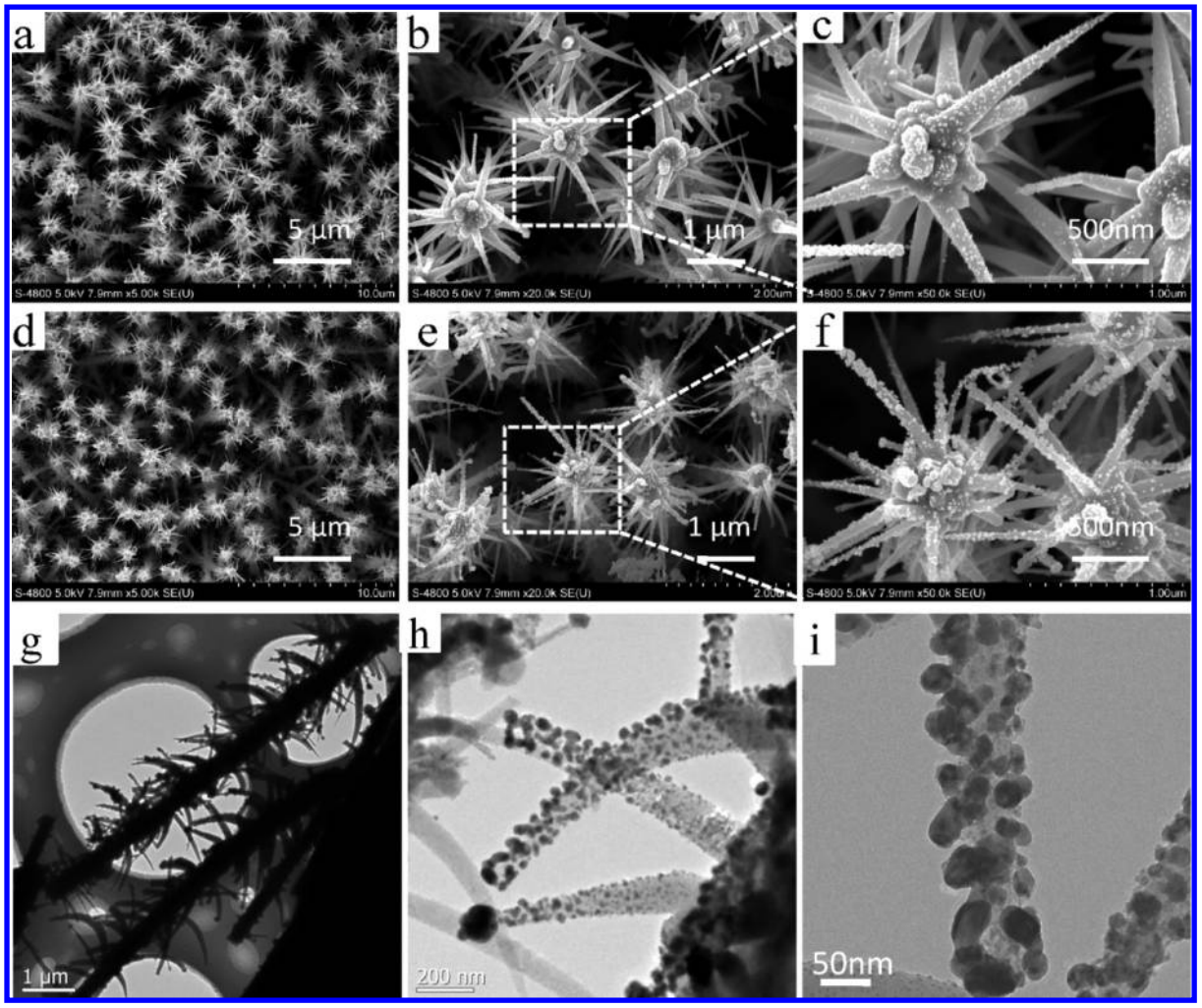

Figure 4. SEM and TEM images of the Ag decorated ZnO/Si nanomace arrays by using different concentrations of $AgNO_3$ for 1 min. (a,b,c) 5×10^{-5} M, (d,e,f) 5×10^{-4} M at different magnifications. Images g, h, and i represent different magnifications of TEM images in the concentration of 5×10^{-4} M.

Si nanoneedles branches (Figure 3c). From Figure 3d–f, the length of the branches was adjustable from 610 ± 120 to 1150 ± 240 nm. The results revealed that the increase of length of the Si nanoneedles accompanied by the increase of deposition duration, which provided a new opportunity to adjust the structure of the branched scaffolds.

3.2. AgNPs Decorated 3D ZnO/Si Nanomace Arrays. According to previous research, the optimization of AgNPs in size, shape, and composition is critical to the improvement of sensitivity and reproducibility of SERS substrates.[49−51] Here, the AgNPs are successfully embedded on the surface of Si nanoneedle branches via a convenient galvanic displacement. In this process, Si nanoneedles act as reducing agents, and AgNPs are immobilized by an oxidation−reduction mechanism in the solution.[52,53] Figure 4 shows the representative SEM and TEM images of the ordered nanomace arrays whose branches (viz Si nanoneedles) are decorated with AgNPs in different initial silver nitrate ($AgNO_3$) concentrations. Obviously, the size of AgNPs increases with increasing silver ions concentrations (Figure 4c,f). As expected, a higher silver ions concentration will cause bigger AgNPs and narrower gap. A rough statistical result displays that the average sizes of AgNPs are approximately 17.0 ± 5.3 and 30.1 ± 9.2 nm for 5×10^{-5} and 5×10^{-4} M concentration, respectively. Based on the fact that different average size of AgNPs will cause much closer gap distance, we estimate that those Ag decorated 3D nanomace arrays could possess different enhancement effectiveness in their SERS detection process. The relationship between the SERS intensity and gap distance (according to Figure 4h,i under TEM) is being studied.

3.3. Characterization of AgNPs Decorated 3D ZnO/Si Nanomace Arrays. To obtain structural characteristics and elements distributions of the as-synthesized 3D hierarchical nanomace arrays, X-ray photoelectron spectroscopy (XPS), X-ray diffraction (XRD), and energy-dispersive spectrometry (EDS) were carried out. As shown in Figure S2 of the Supporting Information, Zn, O, Si, Ag, and C elements could be easily found, and their binding energies in the XPS spectra were calibrated by C 1s (284.8 eV). Furthermore, three sets of diffraction peaks were observed in XRD, which indicates that the prepared nanomace arrays consist of the phases ZnO, Si, and Ag. The sharp diffraction peak at 34.4°, corresponding to (002) plane of ZnO crystal, is very strong and dominant in the XRD spectrum. It not only reveals the intense *c*-axis oriented growth of ZnO nanorods but also reflects the alignment of the ZnO nanorod array perpendicular to the substrate (the results is consistent with the SEM images). Figure 5a shows a selected area for the elemental mapping by EDS, and Figure 5b–e

DOI: 10.1021/am507857x
ACS Appl. Mater. Interfaces 2015, 7, 5725−5735

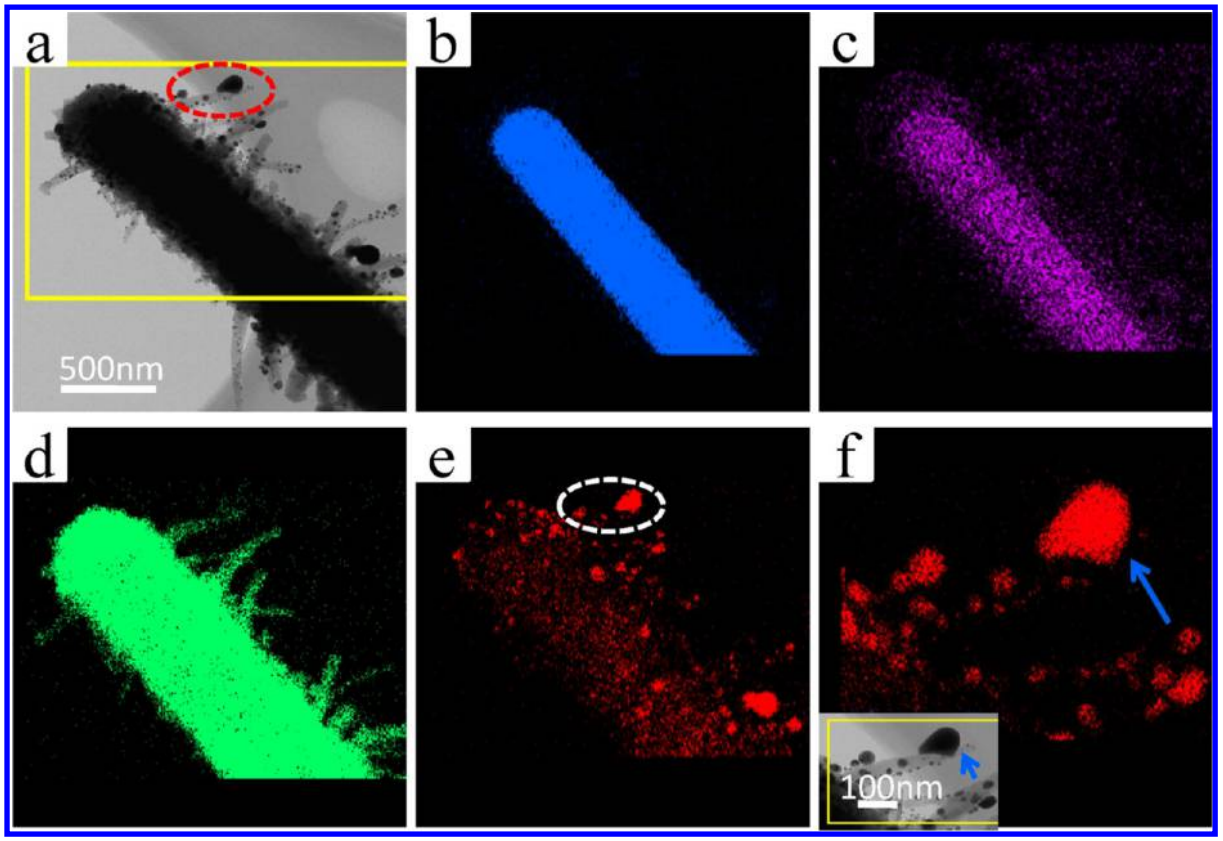

Figure 5. (a) Selected image of the ZnO/Si/Ag hierarchical nanomace arrays for the EDS mapping analysis. The corresponding elemental mapping images for Zn, O, Si, and Ag are presented in panels b, c, d, and e, respectively. (f) Magnification of elemental mapping image for single AgNP and (inset) selected image of single nanoneedle in red circle.

presents the Zn, O, Si, and Ag mappings, respectively. As expected, the element of Zn (Figure 5b) and O (Figure 5c) drops in the middle of sample region, which represents the backbones of ZnO. The Si signals (Figure 5d) are collected from the surface of backbones and nanoneedles which is attributed to the formation of ZnO/Si core−shell nanostructure and Si nanoneedles. Also, the distribution of Ag (Figure 5e) is homogeneous on the surface of the Si nanoneedles and backbones. A magnification of the elemental mapping image for a single Ag nanoparticle is exhibited in Figure 5f. The results indicate again that the ZnO/Si 3D nanomace arrays have been fabricated successfully by PECVD and AgNPs have also been decorated perfectly for SERS application.

Previous research has indicated that the SERS excitation would become most efficient when the laser excitation wavelength coincides with the maximum plasmon absorption wavelength.[54] To understand and optimize the SERS response of the as-prepared AgNPs decorated ZnO/Si nanomace arrays, the UV−visible absorption spectra were measured. As shown in Figure S1 of the Supporting Information, curve i and curve ii present the UV−visible absorption spectra of AgNPs film and AgNPs decorated ZnO nanorods arrays, respectively. Two prominent absorption bands were observed in curve ii, which attributed to the absorption of the metallic AgNPs (peak located at around 300 nm) and characteristic absorption of surface plasmon (resulting from the semiconduction ZnO nanorods arrays, weak peak at 362 nm). However, a strong and broad absorption shoulder band was found at 450−700 nm in the spectrum of AgNPs decorated ZnO/Si nanomace arrays (curve iii). And the broad absorption may be associated with the plasmon coupling of Si nanoneedles and AgNPs. It is clear that the 633 nm wavelength is located in the range of absorption shoulder. Here, a 633 nm laser is chosen instead of a 514 nm laser in order to avoid the effect of resonant Raman scattering (RRS) of R6G, which is excited at 528 nm. The additional enhancement factor (EF) from RRS has been estimated to be 10^5 compared to nonresonant Raman scattering, which may distort the evaluations of EF.[55] It is an overall consideration of the maximum plasmon absorption wavelength and RRS of R6G.

3.4. SERS Detection of R6G Dye. SERS has been proved as a promising method for rapid and sensitive detection of chemicals and biochemicals. To understand whether our nanomace substrates are effective or not for trace detection, the SERS performances of the as-synthesized 3D nanomace substrates were evaluated by using R6G as the probe molecule. R6G is a highly fluorescent dye from the rhodamine family and often used as a tracer dye within water. As shown in Figure 6a, all characteristic peaks of the R6G molecule were observed in the six curves, and these vibration peaks could be assigned to C−H in-plane bending (1181 cm^{-1}), C−O−C stretching (1311 cm^{-1}), and C−C stretching of the aromatic ring (1363, 1511, and 1651 cm^{-1}), respectively.[56] Besides, the peak at 778 cm^{-1} was due to the out-of-plane bending motion of the hydrogen atoms of the xanthene skeleton.[57] Three main characteristic peaks of R6G were observed at 1311, 1363, and 1511 cm^{-1} in these spectra and showing an obvious enhanced effect. Moreover, the Raman spectral intensities were decreased by diluting the concentrations of the R6G probe molecule from 10^{-6} to 10^{-16} M. Almost all of its characteristic peaks were

DOI: 10.1021/am507857x
ACS Appl. Mater. Interfaces 2015, 7, 5725−5735

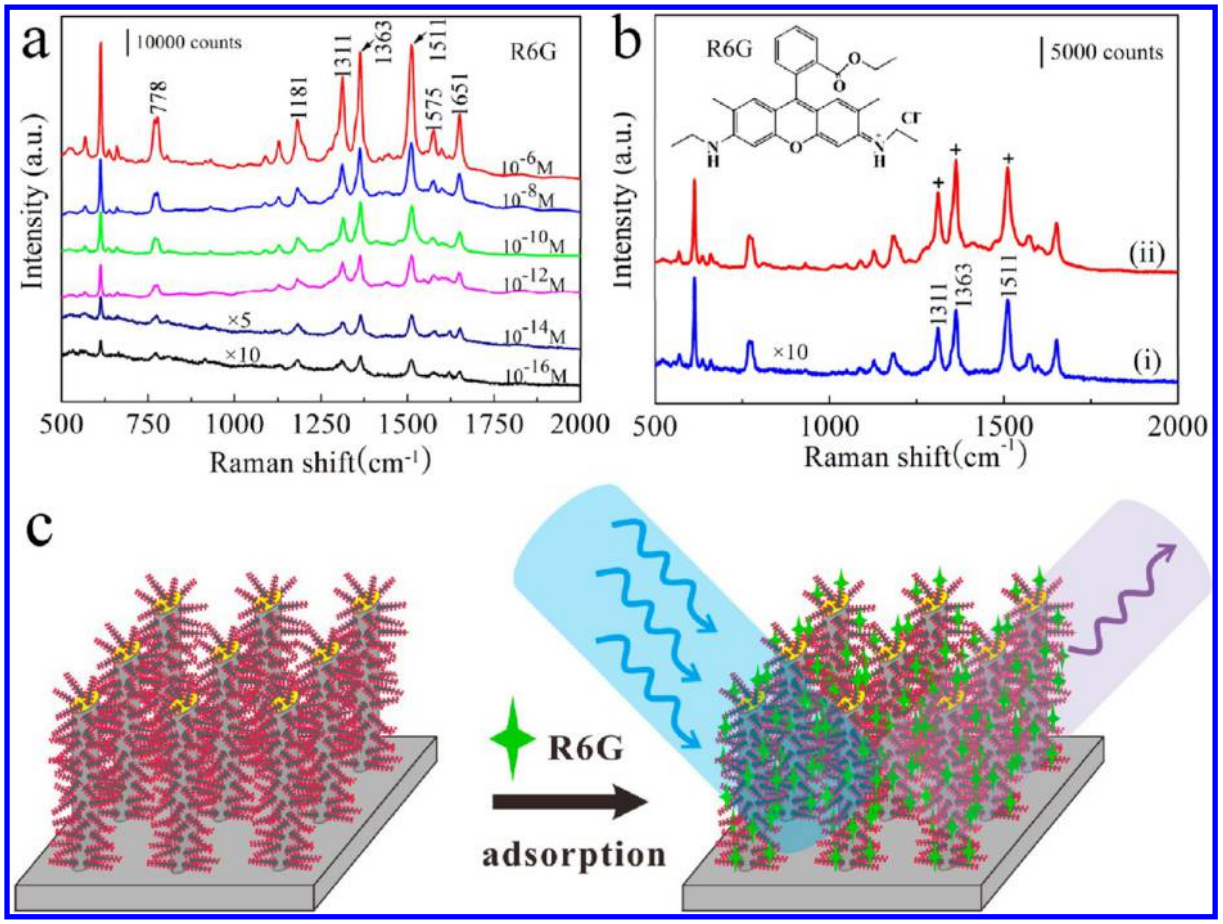

Figure 6. (a) SERS spectra of R6G (incident power was 1.7 mW, the data acquisition time was 10 s) at different concentrations; (b) spectra of R6G. Curve i, 10^{-3} M R6G aqueous solutions as a reference; curve ii, SERS at 10^{-10} M R6G; (c) schematic illustration of the R6G adsorption and its SERS detection.

distinctly observed even when the R6G concentration was down to 10^{-16} M, demonstrating the high sensitivity of this 3D nanomace arrays. According to the previous study,[58] the sensitivity of a SERS substrate is characterized by the EF which is defined by the expression EF = $(I_{surface}/I_{solution}) \times (N_{solution}/N_{surface})$, where $N_{solution}$ and $N_{surface}$ are the numbers of molecules probed in a reference solution and on nanomaces SERS substrates, and $I_{solution}$ and $I_{surface}$ are the signal intensities of the reference solution and the SERS substrate, respectively.

Figure 6b exhibits the spectra comparison result of the SERS substrates and the reference solution. The characteristic band at 1363 cm^{-1} was chosen for the EF estimation. The SERS signal intensities ($I_{surface}$) were about 14980 for nanomace SERS substrates and the $I_{solution}$ were about 1079 in a reference solution. The number of the detected molecule can be estimated by $N_{surface} = (N_A C V_{solution}/S_{disp}) \times S_{laser}$, where N_A is the Avogadro constant, C is the molar concentration of the solution, $V_{solution}$ is the volume of the droplet, S_{disp} is the dispersed area on the substrate, and S_{laser} is the size of the laser spot. In our experiments, 10 μL of a 1×10^{-10} M R6G aqueous solution was dropped onto 10 × 10 mm nanomaces substrates and dispersed to an area of ~12.6 mm^2. The probed molecules on nanomaces substrates are assumed to distribute uniformly on the substrates. About 48 R6G molecules were deposited within a 1 μm^2 area, and correspondingly, $N_{surface} \sim 38$ molecules as a rough estimate for nanomace SERS substrates (an effective area of 0.8 μm^2). In comparison, Raman spectra of a 10^{-3} M R6G aqueous solution were measured applying a laser intensity of 1.7 mW. And the effective excitation volume in solution was estimated as ~400 μm^3,[59] to give $N_{solution} \sim 2.4 \times 10^8$ and a normal Raman intensity of ~4.5×10^{-6} counts per R6G molecule. In this way, the EF of 3D hierarchical nanomace arrays can be obtained as high as 8.7×10^7. Furthermore, the rest of two main Raman bands at 1311 and 1511 cm^{-1} were also selected to estimate the EF (8.0×10^7 and 7.0×10^7, respectively). It should be noted that the EF is different when different Raman band or concentration were chosen for estimation. But those EFs were with the same order of magnitude.

The EF value obtained here were in agreement with those previously reported literature (10^6–10^{10}).[60] And it was about 10^4 times higher than that of AgNPs on planar substrates (the EF of AgNPs on planar Si substrate was ~1.05×10^4). The mechanism was complicated involving the following aspect in our experiments. First, the combination of AgNPs with Si nanoneedles could lead to a strong interaction of exciton–plasmon and yield enhanced localized surface electrical field.[61] Second, close packed AgNPs are decorated on the Si nanoneedles readily, which generate a high density of hotspots by AgNPs aggregation and increase the electromagnetic field significantly.[62] Next, Si nanoneedles are also regarded as "nanoantenna" owing to a shrinking Au remnant droplet at the end of nanoneedles.[63] Finally, abundant Si nanoneedles scaffolds and huge surface area accelerate more probe molecule

DOI: 10.1021/am507857x
ACS Appl. Mater. Interfaces 2015, 7, 5725–5735

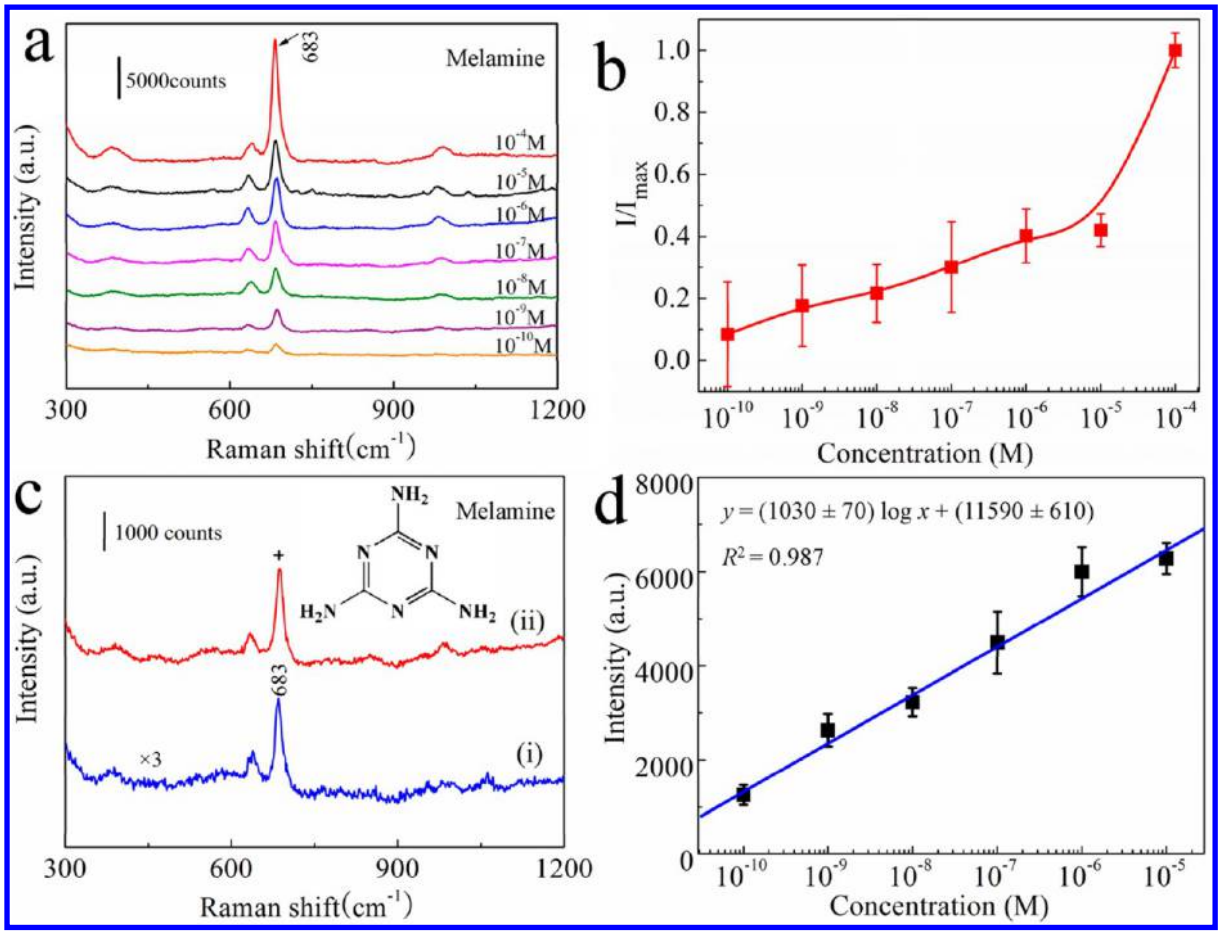

Figure 7. (a) SERS spectra of melamine (incident power was 1.7 mW, the data acquisition time was 10 s) at different concentrations; (b) relationship between the normalized peak intensity and the melamine concentration; (c) Raman spectra of melamine. Curve i, 10^{-3} M melamine aqueous solutions as a reference; curve ii, SERS at 10^{-9} M melamine; (d) linear relationships between SERS intensity and melamine concentrations at band 683 cm^{-1}.

adsorption. Therefore, it is not surprising that the as-prepared nanomace arrays result in considerable enhancement of the Raman scattering intensity.

3.5. Practical Analysis of Melamine. Melamine may be the most notorious one that was implicated in milk and infant formula, because it can lead to kidney disease and even mortality in infants. To demonstrate whether our 3D nanomace SERS substrate is highly sensitive for melamine detection or not, we prepared melamine aqueous solutions with different concentrations from 10^{-4} to 10^{-10} M and introduced them to the nanomace arrays for SERS measurement. Figure 7a presents the typical SERS spectra of 3D nanomace arrays under different melamine concentrations, and the Raman spectral intensities were decreased by diluting the melamine aqueous solutions. The characteristic peaks of melamine were clearly observed in these spectra at 683 cm^{-1} which was assigned to the in-plane ring breathing II mode.[64] A distinct characteristic peak was observed even when the melamine concentration was down to 10^{-10} M, demonstrating the high sensitivity of the as-prepared 3D nanomace arrays. The increasing trend of SERS intensity with melamine concentration was further summarized in Figure 7b for quantitative melamine sensing. And the intense SERS peak at 683 cm^{-1} in the spectra has been used as a calibration band. A gradual increase in SERS intensity was observed as the melamine concentration increasing. Above 10^{-5} M, a step response was observed in signal intensity, indicating a stronger response to high concentration of melamine. The calibration curve in the concentration ranging from10^{-10} to 10^{-5} M is shown in Figure 7d. The linear equation is determined as $y = (1030 \pm 70) \log x + (11590 \pm 610)$, $(10^{-10} < x < 10^{-5})$ with the correlation coefficient $R^2 = 0.987$, where y is the SERS intensity and x is the concentration of melamine. Based on this study, the linear equation could provide an opening for practical analysis of trace melamine in melamine-contaminated products.

The EF value of melamine (which adsorbed on the 3D nanomace arrays) was measured as above. As illustrated in Figure 7c, the SERS signal intensities, $I_{surface}$, were about 2656 (spectra ii) for nanomace SERS substrates and the $I_{solution}$ were about 854 (spectra i) in a reference solution. Thus, the ratio $I_{surface}/I_{solution}$ could be calculated to be about 3.24 from the intensity of the peaks at 683 cm^{-1}. According to the formula mentioned above, the EF value was calculated to be about 2.04×10^6, which indicating the detection of trace melamine could be performed using this 3D nanomace arrays.

In addition to the high sensitivity and EF value, the reproducibility of substrate SERS signal is also an important parameter. To test the reproducibility (substrate uniformity) of our substrate, SERS spectra of melamine molecules with a concentration of 10^{-8} M from six random-selected places on the Ag decorated 3D nanomace arrays were collected under identical experimental conditions. As shown in Figure 8a, these

DOI: 10.1021/am507857x
ACS Appl. Mater. Interfaces 2015, 7, 5725−5735

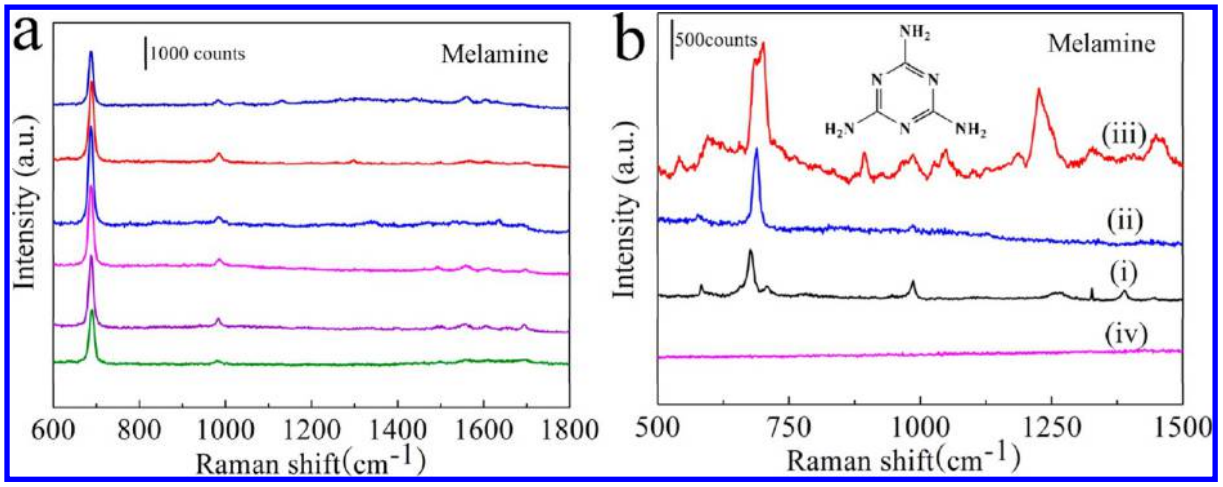

Figure 8. (a) Reproducibility of the SERS signals (incident power was 1.7 mW, the data acquisition time was 5 s, 10^{-8} M melamine) at six random sites; (b) SERS spectra of melamine at different conditions, curve i, melamine powder; curve ii, melamine aqueous solution (10^{-9} M); curve iii, melamine-contaminated milk sample (10^{-9} M); curve iv, pure milk without melamine as a reference.

SERS signals exhibited good similarity. For the peak at 683 cm^{-1}, the relative standard deviation (RSD) of the SERS intensity is about 17%. This low RSD indicates that the structure and surface property of our substrate is rather uniform.

Curves i and ii in Figure 8b represent the Raman spectra of melamine powder and melamine aqueous solution, respectively. The SERS intensity at 675 cm^{-1} due to the in-plane deformation of the triazine ring with the vibration of the amino nitrogen atoms.[64] For practical applications, there will be several nutrient ingredients in melamine-contaminated milk sample, which disturbed the detection of melamine. As a result, we tested the selectivity of our SERS probe in the presence of melamine-contaminated commercial milk sample. Obviously, more peaks and a large background were observed in melamine-contaminated commercial milk (curve iii compared with the melamine aqueous solution (curve ii), and pure milk (curve iv)). This is likely due to the nutrient ingredients (including the protein, carbohydrates, and grease) added to commercial milk, which showed the impurities sensing. Surprisingly, we still obtained tremendous SERS intensity of the characteristic Raman peak of melamine at 683 cm^{-1}, which does not interfere with the detection of melamine in milk and shows excellent selectivity over other nutrient ingredients. Therefore, it is a convenient detection for melamine without separating the nutrient ingredients from milk. Our experimental results clearly demonstrate that our SERS substrates can be used for the detection of melamine from melamine simulating solutions to melamine-contaminated milk sample. Detailed and thorough research about the Raman spectroscopy and melamine-contaminated milk sample is now under way.

4. CONCLUSION

In summary, we have successfully fabricated a unique 3D AgNPs decorated ZnO/Si heterostructured nanomace arrays. It is shown that the preparation consists of two steps: the graft of Si nanoneedles onto ZnO nanorod arrays and the subsequent decoration of the AgNPs. The as-fabricated substrates were applied for the detection of R6G molecules, with a Raman enhancement factors up to 8.7×10^7. This would significantly enhance the sensitivity of the SERS substrates and push the detection limit down to 10^{-16} M. Furthermore, the applicability of the prepared substrates for the detection of melamine in aqueous solutions (from 10^{-4} to 10^{-10} M) was demonstrated with satisfactory results. Owning to the excellent selectivity over other nutrient ingredients, the detection of melamine residual in pure milk was carried out successfully, and the results indicated that the prepared 3D nanomace substrates might be useful in many chemical and biological analysis fields.

■ ASSOCIATED CONTENT

Supporting Information

UV−visible absorption spectra, XRD, XPS data and statistical intensities distributions of the different R6G concentrations. This material is available free of charge via the Internet at http://pubs.acs.org.

■ AUTHOR INFORMATION

Corresponding Authors

*Y. Zhao. E-mail: yxzhao@mail.xjtu.edu.cn.
*K. Xu. E-mail: kwxu@mail.xjtu.edu.cn.
*D. Ma. E-mail: madayan@mail.xjtu.edu.cn.

Notes

The authors declare no competing financial interest.

■ ACKNOWLEDGMENTS

This research was financially supported by Key Project of the Chinese National Programs for Fundamental Research and Development (Grant No. 2010CB631002), the National Natural Science Foundation of China (Grant Nos. 21475102 and 51171145), the Natural Science Foundation of Shanxi Province (Grant No. 2013JQ2017), and the Fundamental Research Funds for the Central Universities.

■ REFERENCES

(1) Fleischmann, M.; Hendra, P.; McQuillan, A. Raman Spectra of Pyridine Adsorbed at a Silver Electrode. *Chem. Phys. Lett.* **1974**, *26*, 163−166.

(2) Yamazoe, S.; Naya, M.; Shiota, M.; Morikawa, T.; Kubo, A.; Tani, T.; Hishiki, T.; Horiuchi, T.; Suematsu, M.; Kajimura, M. Large-Area Surface-Enhanced Raman Spectroscopy Imaging of Brain Ischemia by Gold Nanoparticles Grown on Random Nanoarrays of Transparent Boehmite. *ACS Nano* **2014**, *8*, 5622−5632.

(3) Samanta, A.; Maiti, K. K.; Soh, K. S.; Liao, X.; Vendrell, M.; Dinish, U.; Yun, S. W.; Bhuvaneswari, R.; Kim, H.; Rautela, S.

DOI: 10.1021/am507857x
ACS Appl. Mater. Interfaces 2015, 7, 5725−5735

Ultrasensitive near-Infrared Raman Reporters for SERS-Based in Vivo Cancer Detection. *Angew. Chem., Int. Ed.* **2011**, *50*, 6089−6092.
(4) Lin, L.; Tian, X.; Hong, S.; Dai, P.; You, Q.; Wang, R.; Feng, L.; Xie, C.; Tian, Z. Q.; Chen, X. A Bioorthogonal Raman Reporter Strategy for SERS Detection of Glycans on Live Cells. *Angew. Chem.* **2013**, *125*, 7407−7412.
(5) Kodiyath, R.; Malak, S. T.; Combs, Z. A.; Koenig, T.; Mahmoud, M. A.; El-Sayed, M. A.; Tsukruk, V. V. Assemblies of Silver Nanocubes for Highly Sensitive SERS Chemical Vapor Detection. *J. Mater. Chem. A* **2013**, *1*, 2777−2788.
(6) Xia, X.; Rycenga, M.; Qin, D.; Xia, Y. A Silver Nanocube on a Gold Microplate as a Well-Defined and Highly Active Substrate for SERS Detection. *J. Mater. Chem. C* **2013**, *1*, 6145−6150.
(7) Wang, Y.; Zhang, X.; Gao, P.; Shao, Z.; Zhang, X.; Han, Y.; Jie, J. Air Heating Approach for Multilayer Etching and Roll-to-Roll Transfer of Silicon Nanowire Arrays as SERS Substrates for High Sensitivity Molecule Detection. *ACS Appl. Mater. Interfaces* **2014**, *6*, 977−984.
(8) Shanmukh, S.; Jones, L.; Driskell, J.; Zhao, Y.; Dluhy, R.; Tripp, R. A. Rapid and Sensitive Detection of Respiratory Virus Molecular Signatures Using a Silver Nanorod Array SERS Substrate. *Nano Lett.* **2006**, *6*, 2630−2636.
(9) Ros, I.; Placido, T.; Amendola, V.; Marinzi, C.; Manfredi, N.; Comparelli, R.; Striccoli, M.; Agostiano, A.; Abbotto, A.; Pedron, D. SERS Properties of Gold Nanorods at Resonance with Molecular, Transverse, and Longitudinal Plasmon Excitations. *Plasmonics* **2014**, *9*, 581−593.
(10) Zhang, Y.; Qian, J.; Wang, D.; Wang, Y.; He, S. Multifunctional Gold Nanorods with Ultrahigh Stability and Tunability for in Vivo Fluorescence Imaging, SERS Detection, and Photodynamic Therapy. *Angew. Chem., Int. Ed.* **2013**, *52*, 1148−1151.
(11) Liu, Z.; Cheng, L.; Zhang, L.; Yang, Z.; Liu, Z.; Fang, J. Sub-100 nm Hollow Au-Ag Alloy Urchin-Shaped Nanostructure with Ultrahigh Density of Nanotips for Photothermal Cancer Therapy. *Biomaterials* **2014**, *35*, 4099−4107.
(12) Bi, L.; Rao, Y.; Tao, Q.; Dong, J.; Su, T.; Liu, F.; Qian, W. Fabrication of Large-Scale Gold Nanoplate Films as Highly Active SERS Substrates for Label-Free DNA Detection. *Biosens. Bioelectron.* **2013**, *43*, 193−199.
(13) Dendisová, M.; Havránek, L. S.; Ončák, M.; Matejka, P. In Situ SERS Study of Azobenzene Derivative Formation from 4-Amino-benzenethiol on Gold, Silver, and Copper Nanostructured Surfaces: What is the Role of Applied Potential and Used Metal? *J. Phys. Chem. C* **2013**, *117*, 21245−21253.
(14) Dai, Z.; Mei, F.; Xiao, X.; Liao, L.; Fu, L.; Wang, J.; Wu, W.; Guo, S.; Zhao, X.; Li, W. Rings of Saturn-Like" Nanoarrays with High Number Density of Hot Spots for Surface-Enhanced Raman Scattering. *Appl. Phys. Lett.* **2014**, *105*, 033515.
(15) Cai, W.; Tang, X.; Yang, L.; Wang, X. Facile Fabrication of Leafy Spikes-Like Silver Dendrite Crystals for SERS Substrate. *Mater. Res. Bull.* **2013**, *48*, 4125−4133.
(16) Tang, X.; Cai, W.; Yang, L.; Liu, J. Highly Uniform and Optical Visualization of SERS Substrate for Pesticide Analysis Based on Au Nanoparticles Grafted on Dendritic α-Fe_2O_3. *Nanoscale* **2013**, *5*, 11193−11199.
(17) Song, H. M.; Deng, L.; Khashab, N. M. Intracellular Surface-Enhanced Raman Scattering (SERS) with Thermally Stable Gold Nanoflowers Grown from Pt and Pd Seeds. *Nanoscale* **2013**, *5*, 4321−4329.
(18) Nhung, T. T.; Bu, Y.; Lee, S.-W. Facile Synthesis of Chitosan-Mediated Gold Nanoflowers as Surface-Enhanced Raman Scattering (SERS) Substrates. *J. Cryst. Growth* **2013**, *373*, 132−137.
(19) Li, Q.; Jiang, Y.; Han, R.; Zhong, X.; Liu, S.; Li, Z. Y.; Sha, Y.; Xu, D. High Surface-Enhanced Raman Scattering Performance of Individual Gold Nanoflowers and Their Application in Live Cell Imaging. *Small* **2013**, *9*, 927−932.
(20) Zhang, L. F.; Zhong, S. L.; Xu, A. W. Highly Branched Concave Au/Pd Bimetallic Nanocrystals with Superior Electrocatalytic Activity and Highly Efficient SERS Enhancement. *Angew. Chem., Int. Ed.* **2013**, *52*, 645−649.
(21) Liu, S.; Yang, M.-Q.; Tang, Z.-R.; Xu, Y.-J. A Nanotree-Like CdS/ZnO Nanocomposite with Spatially Branched Hierarchical Structure for Photocatalytic Fine-Chemical Synthesis. *Nanoscale* **2014**, *6*, 7193−7198.
(22) Tan, Y.; Gu, J.; Xu, W.; Chen, Z.; Liu, D.; Liu, Q.; Zhang, D. Reduction of CuO Butterfly Wing Scales Generates Cu SERS Substrates for DNA Base Detection. *ACS Appl. Mater. Interfaces* **2013**, *5*, 9878−9882.
(23) Tan, Y.; Gu, J.; Xu, L.; Zang, X.; Liu, D.; Zhang, W.; Liu, Q.; Zhu, S.; Su, H.; Feng, C.; Fan, G.; Zhang, D. High-Density Hotspots Engineered by Naturally Piled-Up Subwavelength Structures in Three-Dimensional Copper Butterfly Wing Scales for Surface-Enhanced Raman Scattering Detection. *Adv. Funct. Mater.* **2012**, *22*, 1578−1585.
(24) Albella, P.; Alcaraz de la Osa, R.; Moreno, F.; Maier, S. A. Electric and Magnetic Field Enhancement with Ultra-Low Heat Radiation Dielectric Nanoantennas: Considerations for Surface Enhanced Spectroscopies. *ACS Photonics* **2014**, *1*, 524−529.
(25) Shao, F.; Lu, Z.; Liu, C.; Han, H.; Chen, K.; Li, W.; He, Q.; Peng, H.; Chen, J. Hierarchical Nanogaps within Bioscaffold Arrays as a High-Performance SERS Substrate for Animal Virus Biosensing. *ACS Appl. Mater.Interfaces* **2014**, *6*, 6281−6289.
(26) Tan, Y.; Gu, J.; Zang, X.; Xu, W.; Shi, K.; Xu, L.; Zhang, D. Versatile Fabrication of Intact Three-Dimensional Metallic Butterfly Wing Scales with Hierarchical Sub-micrometer Structures. *Angew. Chem., Int. Ed.* **2011**, *50*, 8307−8311.
(27) Lee, S. Y.; Kim, S.-H.; Kim, M. P.; Jeon, H. C.; Kang, H.; Kim, H. J.; Kim, B. J.; Yang, S.-M. Freestanding and Arrayed Nanoporous Microcylinders for Highly Active 3D SERS Substrate. *Chem. Mater.* **2013**, *25*, 2421−2426.
(28) Chen, M.; Phang, I. Y.; Lee, M. R.; Yang, J. K.W.; Ling, X. Y. Layer-By-Layer Assembly of Ag Nanowires into 3D Woodpile-Like Structures to Achieve High Density "Hot Spots" for Surface-Enhanced Raman Scattering. *Langmuir* **2013**, *29*, 7061−7069.
(29) Md Jani, A. M.; Losic, D.; Voelcker, N. H. Nanoporous Anodic Aluminium Oxide: Advances in Surface Engineering and Emerging Applications. *Prog. Mater. Sci.* **2013**, *58*, 636−704.
(30) Makaryan, T.; Esconjauregui, S.; Gonçalves, M.; Yang, J.; Sugime, H.; Nille, D.; Renganathan, P. R.; Goldberg-Oppenheimer, P.; Robertson, J. Hybrids of Carbon Nanotube Forests and Gold Nanoparticles for Improved Surface Plasmon Manipulation. *ACS Appl. Mater.Interfaces* **2014**, *6*, 5344−5349.
(31) Chen, J.; Yang, L. Synthesis and SERS Performance of a Recyclable SERS Substrate Based on Ag NPs Coated TiO_2 NT Arrays. *Integr. Ferroelectr.* **2013**, *1*, 17−23.
(32) Yang, X.; Zhong, H.; Zhu, Y.; Shen, J.; Li, C. Ultrasensitive and Recyclable SERS Substrate Based on Au-Decorated Si Nanowire Arrays. *Dalton Trans.* **2013**, *42*, 14324−14330.
(33) Liu, K.; Li, D.; Li, R.; Wang, Q.; Pan, S.; Peng, W.; Chen, M. Silver-Decorated ZnO Hexagonal Nanoplate Arrays as SERS-Active Substrates: An Experimental and Simulation Study. *J. Mater. Res.* **2013**, *28*, 3374−3383.
(34) Tan, E.-Z.; Yin, P.-G.; You, T.-T.; Wang, H.; Guo, L. Three Dimensional Design of Large-Scale TiO_2 Nanorods Scaffold Decorated by Silver Nanoparticles as SERS Sensor for Ultrasensitive Malachite Green Detection. *ACS Appl. Mater.Interfaces* **2012**, *4*, 3432−3437.
(35) Dong, J. J.; Zhang, X. W.; Yin, Z. G.; Wang, J. X.; Zhang, S. G.; Si, F. T.; Gao, H. L.; Liu, X. Ultraviolet Electroluminescence from Ordered ZnO Nanorod Array/p-GaN Light Emitting Diodes. *Appl. Phys. Lett.* **2012**, *100*, 171109−171111.
(36) Yuan, J.; Li, H.; Wang, Q.; Zhang, X.; Cheng, S.; Yu, H.; Zhu, X.; Xie, Y. Facile Fabrication of Aligned SnO_2 Nanotube Arrays and Their Field-Emission Property. *Mater. Lett.* **2014**, *118*, 43−46.
(37) Tsai, D. S.; Lin, C. A.; Lien, W. C.; Chang, H. C.; Wang, Y. L.; He, J. H. Ultra-High-Responsivity Broadband Detection of Si Metal-Semiconductor-Metal Schottky Photodetectors Improved by ZnO Nanorod Arrays. *ACS Nano* **2011**, *5*, 7748−7753.

DOI: 10.1021/am507857x
ACS Appl. Mater. Interfaces 2015, 7, 5725−5735

(38) Jiang, C.; Sun, X.; Lo, G.; Kwong, D.; Wang, J. Improved Dye-Sensitized Solar Cells with a ZnO-Nanoflower Photoanode. *Appl. Phys. Lett.* **2007**, *90*, 263501.
(39) Wang, K.; Qian, X.; Zhang, L.; Li, Y.; Liu, H. Inorganic-Organic pn Heterojunction Nanotree Arrays for a High-Sensitivity Diode Humidity Sensor. *ACS Appl. Mater.Interfaces.* **2013**, *5*, 5825−5831.
(40) Su, S.; Wei, X.; Zhong, Y.; Guo, Y.; Su, Y.; Huang, Q.; Lee, S.-T.; Fan, C.; He, Y. Silicon Nanowire-Based Molecular Beacons for High-Sensitivity and Sequence-Specific DNA Multiplexed Analysis. *ACS Nano* **2012**, *6*, 2582−2590.
(41) Song, S.; Liang, Z.; Zhang, J.; Wang, L.; Li, G.; Fan, C. Gold-Nanoparticle-Based Multicolor Nanobeacons for Sequence-Specific DNA Analysis. *Angew. Chem., Int. Ed.* **2009**, *48*, 8670−8674.
(42) Song, S.; Qin, Y.; He, Y.; Huang, Q.; Fan, C.; Chen, H. Y. Functional Nanoprobes for Ultrasensitive Detection of Biomolecules. *Chem. Soc. Rev.* **2010**, *39*, 4234−4243.
(43) Červenka, J.; Ledinský, M.; Stuchlík, J.; Stuchlíková, H.; Bakardjieva, S.; Hruška, K.; Fejfar, A.; Kočka, J. The Structure and Growth Mechanism of Si Nanoneedles Prepared by Plasma-Enhanced Chemical Vapor Deposition. *Nanotechnology* **2010**, *21*, 415604−415610.
(44) Hannon, J.; Kodambaka, S.; Ross, F.; Tromp, R. The Influence of the Surface Migration of Gold on the Growth of Silicon Nanowires. *Nature* **2006**, *440*, 69−71.
(45) Perea, D. E.; Li, N.; Dickerson, R. M.; Misra, A.; Picraux, S. Controlling Heterojunction Abruptness in VLS-Grown Semiconductor Nanowires via in Situ Catalyst Alloying. *Nano Lett.* **2011**, *11*, 3117−3122.
(46) Chang, C.; Hon, M.; Leu, I. Preparation of ZnO Nanorod Arrays with Tailored Defect-Related Characterisitcs and Their Effect on the Ethanol Gas Sensing Performance. *Sens. Actuators, B* **2010**, *151*, 15−20.
(47) Sun, Y.; Fuge, G. M.; Ashfold, M. N. Growth of Aligned ZnO Nanorod Arrays by Catalyst-Free Pulsed Laser Deposition Methods. *Chem. Phys. Lett.* **2004**, *396*, 21−26.
(48) Cheng, C.; Yan, B.; Wong, S. M.; Li, X.; Zhou, W.; Yu, T.; Shen, Z.; Yu, H.; Fan, H. J. Fabrication and SERS Performance of Silver-Nanoparticle-Decorated Si/ZnO Nanotrees in Ordered Arrays. *ACS Appl. Mater.Interfaces.* **2010**, *2*, 1824−1828.
(49) Banholzer, M. J.; Millstone, J. E.; Qin, L.; Mirkin, C. A. Rationally Designed Nanostructures for Surface-Enhanced Raman Spectroscopy. *Chem. Soc. Rev.* **2008**, *37*, 885−897.
(50) Santoro, G.; Yu, S.; Schwartzkopf, M.; Zhang, P.; Vayalil, S. K.; Risch, J. F.H.; Rübhausen, M. A.; Hernández, M.; Domingo, C.; Roth, S. V. Silver Substrates for Surface Enhanced Raman Scattering: Correlation Between Nanostructure and Raman Scattering Enhancement. *Appl. Phys. Lett.* **2014**, *104*, 243107−243111.
(51) Barmi, M. R.; Andreou, C.; Hoonejani, M. R.; Moskovits, M.; Meinhart, C. D. Aggregation Kinetics of SERS-Active Nanoparticles in Thermally Stirred Sessile Droplets. *Langmuir* **2013**, *29*, 13614−13623.
(52) Wang, Y.; Becker, M.; Wang, L.; Liu, J.; Scholz, R.; Peng, J.; Gösele, U.; Christiansen, S.; Kim, D. H.; Steinhart, M. Nanostructured Gold Films for SERS by Block Copolymer-Templated Galvanic Displacement Reactions. *Nano Lett.* **2009**, *9*, 2384−2389.
(53) Gutés, A.; Carraro, C.; Maboudian, R. Silver Dendrites from Galvanic Displacement on Commercial Aluminum Foil as an Effective SERS Substrate. *J. Am. Chem. Soc.* **2010**, *132*, 1476−1477.
(54) Kang, T.; Yoo, S. M.; Yoon, I.; Lee, S. Y.; Kim, B. Patterned Multiplex Pathogen DNA Detection by Au Particle-on-Wire SERS Sensor. *Nano Lett.* **2010**, *10*, 1189−1193.
(55) Ho, C.-C.; Zhao, K.; Lee, T.-Y. Quasi-3D Gold Nanoring Cavity Arrays with High-Density Hot-Spots for SERS Applications via Nanosphere Lithography. *Nanoscale* **2014**, *6*, 8606−8611.
(56) Tiwari, V. S.; Oleg, T.; Darbha, G. K.; Hardy, W.; Singh, J. P.; Ray, P. C. Non-Resonance SERS Effects of Silver Colloids with Different Shapes. *Chem. Phys. Lett.* **2007**, *446*, 77−82.
(57) Tong, P.; Wu, T.; Wang, X.; Zhang, H.; Kang, Y.; Du, Y. A Novel Alternating Least-Squares Method Based on Fixed Region Scanning Evolving Factor Analysis (FRSEFA) and Its Application in Process Monitoring. *Anal. Methods* **2014**, *6*, 7883−7890.
(58) Le Ru, E. C.; Blackie, E.; Meyer, M.; Etchegoin, P. G. Surface Enhanced Raman Scattering Enhancement Factors: a Comprehensive Study. *J. Phys.Chem. C* **2007**, *111*, 13794−13803.
(59) Cai, W. B.; Ren, B.; Li, X. Q.; She, C. X.; Liu, F. M.; Cai, X. W.; Tian, Z. Q. Investigation of Surface-Enhanced Raman Scattering from Platinum Electrodes Using a Confocal Raman Microscope: Dependence of Surface Roughening Pretreatment. *Surf. Sci.* **1998**, *406*, 9−22.
(60) Zhang, Q.; Lee, Y. H.; Phang, I. Y.; Lee, C. K.; Ling, X. Y. Hierarchical 3D SERS Substrates Fabricated by Integrating Photolithographic Microstructures and Self-Assembly of Silver Nanoparticles. *Small* **2014**, *10*, 2703−2711.
(61) Zhang, M.-L.; Yi, C.-Q.; Fan, X.; Peng, K.-Q.; Wong, N.-B.; Yang, M.-S.; Zhang, R.-Q.; Lee, S.-T. A Surface-Enhanced Raman Spectroscopy Substrate for Highly Sensitive Label-Free Immunoassay. *Appl. Phys. Lett.* **2008**, *92*, 043116−043118.
(62) Fan, J. A.; Wu, C.; Bao, K.; Bao, J.; Bardhan, R.; Halas, N. J.; Manoharan, V. N.; Nordlander, P.; Shvets, G.; Capasso, F. Self-Assembled Plasmonic Nanoparticle Clusters. *Science* **2010**, *328*, 1135−1138.
(63) Galopin, E.; Barbillat, J.; Coffinier, Y.; Szunerits, S.; Patriarche, G.; Boukherroub, R. Silicon Nanowires Coated with Silver Nanostructures as Ultrasensitive Interfaces for Surface-Enhanced Raman Spectroscopy. *ACS Appl. Mater.Interfaces* **2009**, *1*, 1396−1403.
(64) Kim, A.; Barcelo, S. J.; Williams, R. S.; Li, Z. Melamine Sensing in Milk Products by Using Surface Enhanced Raman Scattering. *Anal. Chem.* **2012**, *84*, 9303−9309.

DOI: 10.1021/am507857x
ACS Appl. Mater. Interfaces 2015, 7, 5725−5735